J. Biochem. **137**, 643–652 (2005)
DOI: 10.1093/jb/mvi079

Effects of Mutation at Methionine-42 of *Escherichia coli* Dihydrofolate Reductase on Stability and Function: Implication of Hydrophobic Interactions

Eiji Ohmae[1], Yukari Fukumizu[1], Masahiro Iwakura[2] and Kunihiko Gekko[1,*]

[1]Department of Mathematical and Life Sciences, Graduate School of Science, Hiroshima University, Higashi-Hiroshima 739-8526; and [2]National Institute of Advanced Industrial Science and Technology (AIST), Tsukuba 305-8566

Received January 7, 2005; accepted March 14, 2005

Methionine-42, distal to the active site of *Escherichia coli* dihydrofolate reductase, was substituted by site-directed mutagenesis with 14 amino acids (Ala, Cys, Glu, Gln, Gly, His, Ile, Leu, Pro, Ser, Thr, Trp, Tyr, and Val) to elucidate its role in the stability and function of this enzyme. Far-ultraviolet circular dichroism spectra of these mutants showed a distinctive negative peak at around 230 nm beside 220 nm, depending on the hydrophobicity of the amino acids introduced. The fluorescence intensity also increased in an order similar to that of the amino acids. These spectroscopic data suggest that the mutations do not affect the secondary structure, but strongly perturb the exciton coupling between Trp47 and Trp74. The free energy of urea unfolding, $\Delta G°_u$, increased with increases in the side-chain hydrophobicity in the range 2.96–6.40 kcal·mol^{-1}, which includes the value for the wild-type enzyme (6.08 kcal·mol^{-1}). The steady-state kinetic parameters, K_m and k_{cat}, also increased with increases in the side-chain hydrophobicity, with the M42W mutant showing the largest increases in K_m (35-fold) and k_{cat} (4.3-fold) compared with the wild-type enzyme. These results demonstrate that site 42 distal to the active site plays an important role in the stability and function of this enzyme, and that the main effect of the mutations is to modify of hydrophobic interactions with the residues surrounding this position.

Key words: dihydrofolate reductase, enzyme function, hydrophobic interaction, mutation at methionine-42, structural stability.

Abbreviations: CD, circular dichroism; DHFR, dihydrofolate reductase; DHF, dihydrofolate; THF, tetrahydrofolate; TMP, trimethoprim.

Enzyme function is intimately related to structural fluctuations of a protein molecule to adopt conformations suitable for binding the substrate and cofactor. However, it remains unclear how local structures participate in fluctuations of the whole protein molecule. A novel approach to elucidate the contribution of flexibility on protein function is to clarify the roles of residues distal to the active site that do not participate directly in a catalytic reaction. Knowledge of this contribution should provide a new paradigm for the relationship between structure and function in proteins.

Dihydrofolate reductase (DHFR) from *Escherichia coli* is a typical system for studying structure–fluctuation–function relationships of enzymes. It is a monomeric protein consisting of 159 amino acids with no disulfide bonds, and it catalyzes the NADPH-linked reduction of dihydrofolate (DHF) to tetrahydrofolate (THF). The movie produced by Sawaya and Kraut (*1*) demonstrates how the DHFR molecule actively and cooperatively fluctuates to accommodate the coenzyme and substrate. A high-pressure NMR study revealed the existence of active-site hinge motion including the Met20 loop in solution, which might be directly relevant to function (*2*). We were the first to report that site-directed mutagenesis at Gly121 in a flexible loop significantly influences the stability and function of this enzyme; in particular, the activity of G121V is 240-fold lower than that of wild-type DHFR, despite this position being about 19 Å from the catalytic residue, Asp27 (*3*, *4*). Cameron and Benkovic revealed that G121V has a 200-fold lower hydride-transfer rate and exhibits an additional conformational change step in the Michaelis complex preceding the hydride-transfer step (*5*). Further, we found that site-directed mutagenesis at Gly67 and Ala145 in the other two loops also influences the stability and function of this enzyme (*6*, *7*), and that a double mutation at Gly67 and Gly121, whose α-carbons are mutually separated by 27.7 Å, has nonadditive effects on stability and function (*8*). Single amino acid substitutions at these positions clearly affect the adiabatic compressibility (volume fluctuation) (*9*) and amide hydrogen–deuterium exchange (*10*). These observations indicate that residues distal to the active site are coupled to fluctuations of the structure in solution, a detailed knowledge of which may be crucial to understanding reaction mechanisms.

Recently, Rajagopalan *et al*. showed that while the reaction kinetics of the M42F mutant do not deviate from the wild-type behavior, the forward hydride-transfer rate is 41-fold lower for the M42W mutant (*11*). Double mutations at sites 42 and 121 produced only small changes in

*To whom correspondence should be addressed. Fax: +81-82-424-7387, E-mail: gekko@sci.hiroshima-u.ac.jp

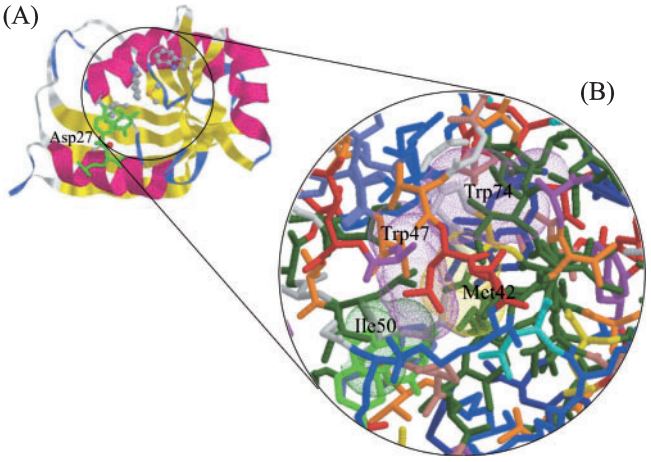

Fig. 1. **The overall structure (A) and an expanded picture around Met42 (B) of a DHFR-MTX binary complex (B-chain).** Taken from Bolin *et al*. (*35*). Panel A: α-helices (red), β-strands (yellow), and turns (blue). Methotrexate is drawn as a stick model and colored green. Side chains of Asp27, Met42, Trp47, and Trp74 are drawn as ball-and-stick models. Panel B: Side chains of Met42, Trp47, Ile50, and Trp74 are drawn as surface models.

substrate and cofactor binding but synergistically decreased the forward hydride-transfer rates, while the decreases in reverse rates were additive. These results suggest that these distal residues exhibit coupled dynamic motion, but the role of site 42 in function and protein dynamics remains unclear because only limited mutation studies have been preformed (*11*, *12*). Since methionine-42 is highly conserved and its side chain is buried in the hydrophobic core (Fig. 1), it should be important in protein folding as well as in enzyme catalysis. In the present study, therefore, we constructed 14 mutants of methionine-42 for further characterization of its role. The effects of mutations on the structure, stability, and enzyme activity are discussed in terms of the correlation with the characteristics—especially hydrophobicity—of the introduced amino acids.

MATERIALS AND METHODS

Construction of Plasmids and Mutants—The genes of mutants were constructed by PCR mutagenesis. The gene for wild-type DHFR was from pTZwt1-3 (*13*). The following two DNA primers were commonly used to amplify an entire gene with a ribosome binding site, overexpression promoter, and *Bam*HI sites at both ends: 5′-GCGGGGATCCTCTTGACAATTAGTTAACTATTTGTTATAATGTAT-3′ (P35-Bam), 5′-GGGGGATCCTTAACGACGCTCGAGGATTTCGAA-3′ (DHFR-C). Site-directed random mutagenesis was performed using a procedure similar to one described previously (*7*) with appropriate mixed primers for a mutagenic PCR. The resulting genes were inserted into the *Bam*HI site of a vector with a large number of copies, pUC19, which was used to endow *E. coli* HB101 cells with trimethoprim (TMP) resistance. Recombinant plasmids were isolated from colonies on agar plates containing 200 mg·ml^{-1} ampicillin and 10 mg·ml^{-1} TMP. DNA sequences of the *Bam*HI insert of the isolated plasmids were determined and the plasmids with mutant sequences were selected.

Protein Purification—The wild-type and mutant DHFR proteins were purified according to methods described previously (*6*, *7*). The concentration of the wild-type DHFR was determined using a molar extinction coefficient of 31,100 M^{-1}·cm^{-1} at 280 nm (*14*). The concentrations of mutant DHFRs except M42Y and M42W were determined assuming the same molar extinction coefficient since the amino acids that were introduced have either no or negligibly small chromophores. The concentrations of M42Y and M42W were determined using molar extinction coefficients of 32,300 and 34,100 M^{-1}·cm^{-1} at 280 nm, respectively. These values were estimated from the intrinsic fluorescence intensity of tryptophan residues in a 5.7 M urea solution, on the assumption that the mutant DHFRs would be fully unfolded and all tyrosine and tryptophan side chains exposed to the solvent.

Circular Dichroism Spectra—Far-ultraviolet circular dichroism (CD) spectra of the wild-type and mutant DHFRs were measured at 15°C using a Jasco J-720W spectropolarimeter as described previously (*6*–*8*). The solvent conditions were 10 mM potassium phosphate (pH 7.0) containing 0.1 mM EDTA and 0.1 mM dithiothreitol. The protein concentration was maintained at about 20 μM.

Fluorescence Spectra—Fluorescence emission spectra of the wild-type and mutant DHFRs were measured using a Jasco FP-750 spectrofluorometer in the wavelength range of 300 to 450 nm at 15°C, with excitation at 290 nm and a slit width of 5 nm. The solvent conditions were the same as those for the CD measurements. The protein concentration was 0.7–1.0 μM.

Thermal Unfolding—Thermal unfolding of the wild-type and M42V DHFRs was monitored by means of CD measurements at 222 nm using a cell with a light path length of 10 mm. The temperature was increased at a rate of 45°C·h^{-1} using a Jasco PTC-348 Peltier-controlled heat block and monitored by a thermistor sensor placed directly in the sample solution. The protein concentration was 1.0–1.5 μM and the solvent conditions were the same as those for the isothermal measurements. The observed molar ellipticity values, [θ] (300–400 points), of M42V DHFR were directly fitted to the two-state unfolding model, native (N) ⇔ unfolded (U), by nonlinear least-squares regression analysis as follows:

$$[\theta] = \{[\theta]_N + [\theta]_U \exp(-\Delta G_u / RT)\} / \{1 + \exp(-\Delta G_u / RT)\} \quad (1)$$

where ΔG_u is the change in Gibbs free energy with unfolding, R is the gas constant, T is the absolute temperature, and $[\theta]_N$ and $[\theta]_U$ are the molar ellipticities of the native and unfolded forms, respectively. $[\theta]_N$ and $[\theta]_U$ at a given temperature were estimated by assuming the same linear dependence of ellipticity in the transition region as in the pure native (pretransition region) and unfolded (posttransition region) states. The change in free energy with unfolding at temperature T, ΔG_T, was calculated as follows

$$\Delta G_T = \Delta H_m + \Delta C_p (T - T_m) - T \{(\Delta H_m / T_m) + \Delta C_p \ln (T / T_m)\} \quad (2)$$

where T_m is the midpoint temperature of the transition, ΔH_m is the change in enthalpy with unfolding at T_m, and ΔC_p is the change in heat capacity with unfolding. In this equation, ΔC_p is assumed to be independent of temperature.

Thermal unfolding of the M42V DHFR was also monitored by fluorescence measurements as described previously (*15*). The solvent conditions were the same as those for the CD measurements. The protein concentration was 0.5 μM.

Equilibrium Unfolding—Equilibrium unfolding of DHFRs in the presence of urea (ultrapure product from ICN Biomedicals) was monitored by means of CD measurements at 222 nm and 15°C with a Jasco J-720W spectropolarimeter as described previously (*6–8*). The solvent conditions were 10 mM potassium phosphate (pH 7.0) containing 0.1 mM EDTA and 0.1 mM dithiothreitol. The protein concentration was maintained at about 20 μM. All samples were fully equilibrated at each denaturant concentration before the CD spectra were measured. The observed molar ellipticity values, [θ] (30–40 points), were fitted directly to the two-state unfolding model as described above (Eq. 1). The change in free energy with unfolding, ΔG_u, was assumed to be linearly dependent on the urea concentration (*16*):

$$\Delta G_u = \Delta G^\circ_u + m\ [\text{urea}] \quad (3)$$

where ΔG°_u is the change in free energy with unfolding in the absence of a denaturant, and the slope, m, is a parameter reflecting the cooperativity of the transition. The urea concentration at the midpoint of the transition ($\Delta G^\circ_u = 0$) was defined as C_m.

Steady-State Kinetics—The steady-state kinetics of the enzyme reaction were studied spectrophotometrically using a Jasco V-560 spectrophotometer at 25°C as described previously (*6–8*). The concentrations of DHF (Sigma) and NADPH (Oriental Yeast) were determined spectrophotometrically using molar extinction coefficients of 28,000 $M^{-1}\cdot cm^{-1}$ at 282 nm and 6,200 $M^{-1}\cdot cm^{-1}$ at 339 nm, respectively (*17*). The enzyme concentrations were determined by the methotrexate titration method to eliminate the effects of denatured species that may be produced during storage. The buffer used was 33 mM succinic acid containing 44 mM imidazole and 44 mM diethanolamine, with pH adjusted to 7.0 with acetic acid or tetraethylammonium hydroxide. The Michaelis constant (K_m) and the rate constant of catalysis (k_{cat}) were measured for various concentrations of DHF (0.3–20 μM) at a saturated concentration of NADPH (60 μM). The DHF concentration was extended to 130 μM for M42W because its K_m was very high. The final concentrations of the enzymes were 0.5–1.5 nM. The enzyme solutions were preincubated with NADPH for 8 min to eliminate the hysteresis effect (*18*), and the reaction was started by adding DHF to the preincubated mixture. The initial velocities (v) of the enzyme reaction were calculated from the time course of absorbance at 340 nm using a differential molar extinction coefficient of 11,800 $M^{-1}\cdot cm^{-1}$ (*19*). The K_m and k_{cat} values were determined using the following equation by nonlinear least-squares analysis:

$$v = (k_{cat}\ [E]\ [S]) / (K_m + [S]) \quad (4)$$

where [E] is the enzyme concentration and [S] is the initial substrate concentration.

Equilibrium Dissociation Constants—The equilibrium dissociation constants, K_d, between ligands (folate or NADPH) and the wild-type or M42W DHFRs were measured by quenching the intrinsic tryptophan fluorescence as a function of ligand concentration using a Jasco FP-750 spectrofluorometer at 25°C. The solvent conditions were 10 mM potassium phosphate (pH 7.0) containing 0.1 mM EDTA and 0.1 mM dithiothreitol. The protein concentration was 3.0–4.5 μM. Observed fluorescence intensities at 345 nm, F, were plotted against the ligand concentrations and fitted to the following equation using nonlinear least-squares analysis:

$$F = F_0P + \Delta F\ [(P + L + K_d) - \{(P + L + K_d)^2 - 4PL\}^{0.5}] / 2 \quad (5)$$

where F_0 is the molar fluorescence intensity of protein without ligand, ΔF is the molar fluorescence intensity change between the protein–ligand complex and free protein, and P and L are the concentrations of the protein and ligand, respectively.

RESULTS

Circular Dichroism Spectra—Figure 2 shows far-ultraviolet CD spectra of the wild-type and mutant DHFRs at 15°C and pH 7.0. The wild type exhibits a negative peak of –8,500 $deg\cdot cm^2\cdot dmol^{-1}$ at around 220 nm, which is consistent with previous data (*6–8*). However, the CD spectra of all mutants (except for M42P) differ greatly from that of the wild type: their intensities are higher at around 230 nm and lower at around 220 nm than those of the wild type. Nonpolar (aliphatic) amino acids significantly increase the peak intensity at 230 nm (Fig. 2A) in the order Pro < wild type < Gly < Ala < Leu < Val < Ile, which is close to the orders of hydrophobicity and volume of the side chains. Polar and acidic amino acids (Cys, Ser, Thr, Gln, and Glu) also enhance the intensity at around 230 nm (Fig. 2B), although their effects are less than those of the nonpolar amino acids. A similar increase in the intensity at around 230 nm was also observed for aromatic amino acids (His, Trp, and Tyr), but their effects are small despite the differing size and hydrophobicity (Fig. 2C). These CD data suggest that the conformation of DHFR is very sensitive to the local structure surrounding site 42.

In order to examine the ligand binding effect on the structure of mutants, the CD spectrum of M42I, which has the highest CD intensity at 230 nm, was measured in the presence of folate at 15°C and pH 7.0. As shown in Fig. 3, increasing folate concentration increased the peak intensity at around 220 nm and decreased it at around 230 nm, with an isoellipticity point at 224 nm. The spectrum for a saturated concentration of folate (100 μM) is very close to that of the wild type. These results suggest that the structure of M42I is shifted to that of the wild type by folate binding.

Fluorescence Spectra—Figure 4 shows fluorescence emission spectra of the wild-type and mutant DHFRs at 15°C and pH 7.0. All mutants except M42Q exhibited a

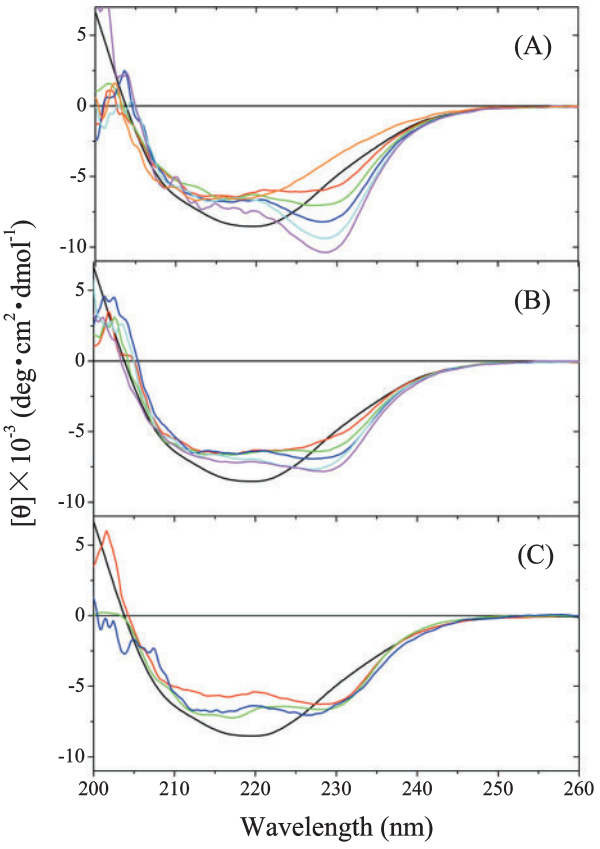

Fig. 2. **Far-ultraviolet circular dichroism spectra of wild-type and mutant DHFRs at 15°C and pH 7.0.** The solvent used was 10 mM potassium phosphate (pH 7.0) containing 0.1 mM EDTA and 0.1 mM dithiothreitol. Panel A: Wild type (black), M42G (red), M42A (green), M42L (blue), M42V (cyan), M42I (magenta), and M42P (orange). Panel B: Wild type (black), M42E (red), M42S (green), M42T (blue), M42C (cyan), and M42Q (magenta). Panel C: Wild type (black), M42H (red), M42W (green), and M42Y (blue).

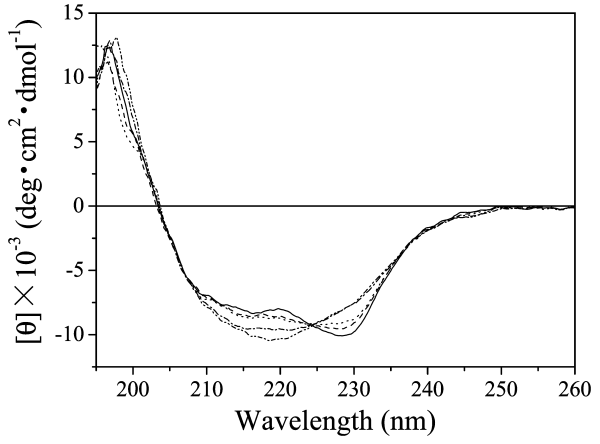

Fig. 3. **Folate concentration dependence of the far-ultraviolet CD spectrum of the M42I DHFR at 15°C and pH 7.0.** The solvent used was 10 mM potassium phosphate (pH 7.0) containing 0.1 mM EDTA and 0.1 mM dithiothreitol. The folate concentrations are indicated as follows: 0 (—), 5 μM (– –), 10 μM (·····), 50 μM (– · –), and 100 μM (– · · –).

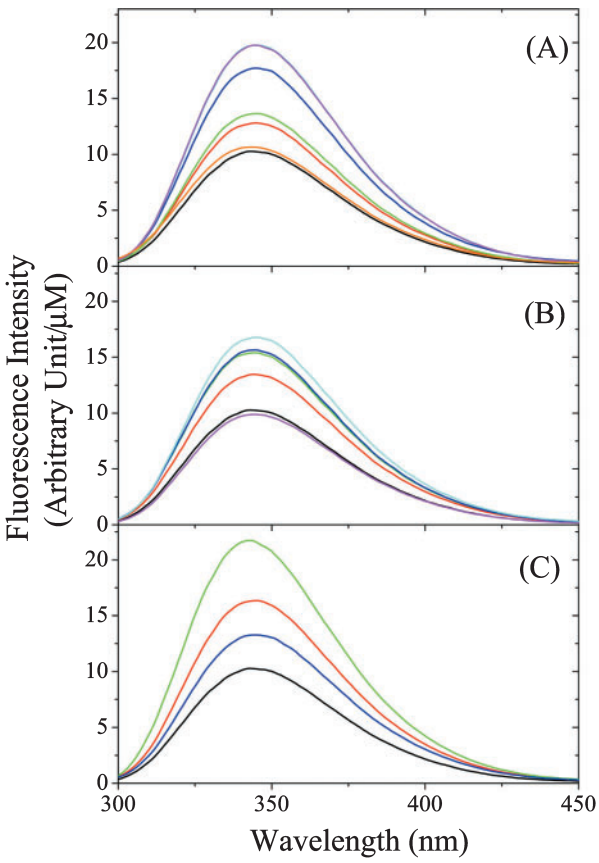

Fig. 4. **Fluorescence spectra of wild-type and mutant DHFRs at 15°C and pH 7.0.** The solvent used was 10 mM potassium phosphate (pH 7.0) containing 0.1 mM EDTA and 0.1 mM dithiothreitol. Panel A: Wild type (black), M42G (red), M42A (green), M42L (blue), M42V (cyan), M42I (magenta), and M42P (orange). Panel B: Wild type (black), M42E (red), M42S (green), M42T (blue), M42C (cyan), and M42Q (magenta). Panel C: Wild type (black), M42H (red), M42W (green), and M42Y (blue).

large increase in fluorescence intensity, but no peak shift. This result suggests that mutations at site 42 enhance the quantum yield of tryptophan residues but do not affect the polarity around them. Of the five tryptophan residues, the most probable candidates for such large changes in the spectrum are Trp47 and Trp74, since Trp74 contributes most strongly to the fluorescence spectrum and the fluorescence of Trp47 is partly quenched in the wild-type DHFR (*15*, *20*). The fluorescence intensity increases in the order wild type < Pro < Gly < Ala < Leu < Val = Ile (Fig. 4A), which is similar to the order of increasing CD intensity at 230 nm (Fig. 2A). The order of the intensity of the polar amino acids, Gln < wild type < Glu < Ser < Thr < Cys (Fig. 4B), is also close to that observed for the CD intensity at around 230 nm (Fig. 2B). Aromatic residues also induce a large increase in fluorescence intensity in the order wild type < Tyr < His < Trp, although no noticeable difference was observed in the CD intensity (Fig. 4C). The high intensity and 2-nm blue shift of the M42W mutant may be partly due to the introduced tryptophan residue, which enhances nonpolarity of the hydrophobic core around the mutation site.

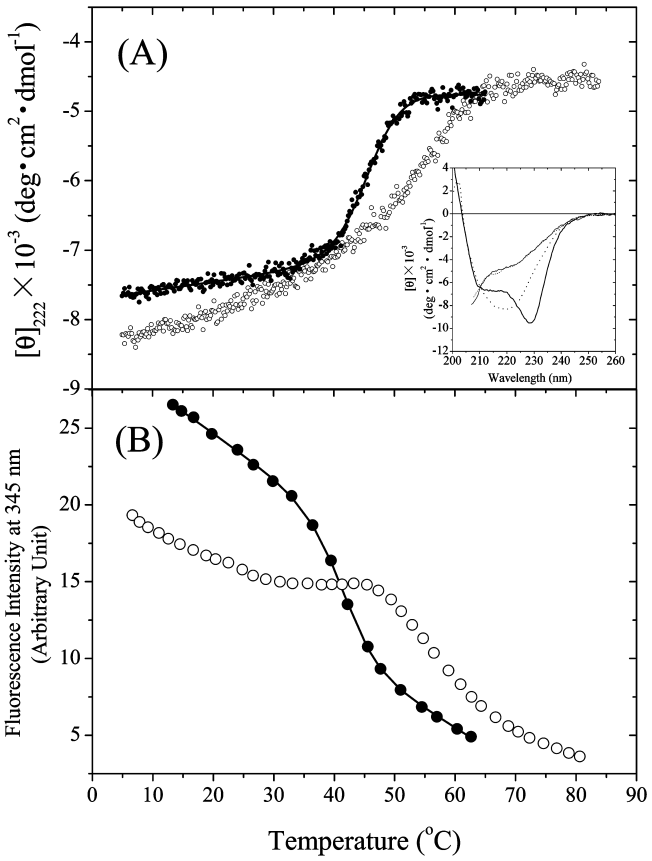

Fig. 5. **Temperature dependence of the CD intensity at 222 nm (A) and the fluorescence intensity at 345 nm (B) of the wild-type and M42V DHFRs at pH 7.0.** The solvent used was 10 mM potassium phosphate (pH 7.0) containing 0.1 mM EDTA and 0.1 mM dithiothreitol: wild type (open circles), M42V (solid circles). Solid lines represent the theoretical fits to a two-state unfolding model (see "MATERIALS AND METHODS"). The inset in panel A shows far-ultraviolet CD spectra of the wild-type and M42V DHFRs at 15 and 80°C: wild type at 15°C (•••), M42V at 15°C (bold thick line), wild type at 80°C (· · ·), M42V at 80°C (thin line).

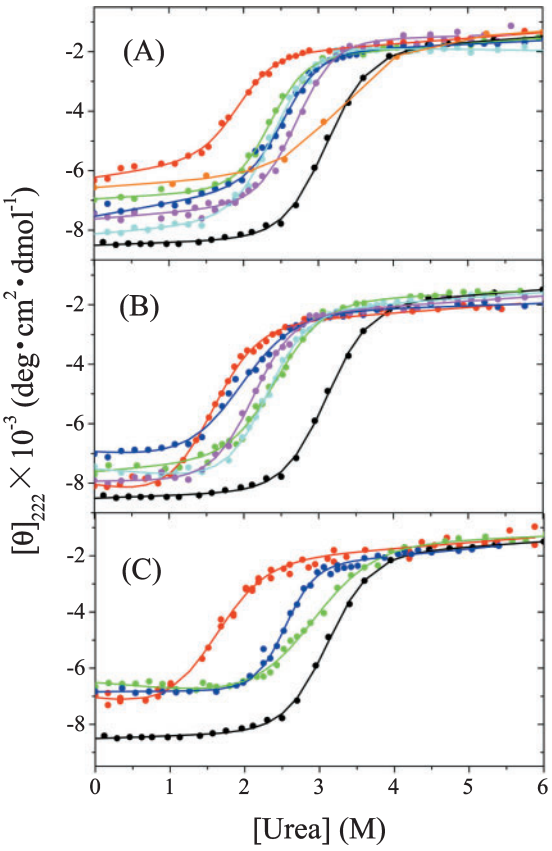

Fig. 6. **Plots of molar ellipticity of the wild-type and mutant DHFRs at 222 nm as a function of urea concentration at 15°C.** The solvent used was 10 mM potassium phosphate (pH 7.0) containing 0.1 mM EDTA and 0.1 mM dithiothreitol. Panel A: Wild type (black), M42G (red), M42A (green), M42L (blue), M42V (cyan), M42I (magenta), and M42P (orange). Panel B: Wild type (black), M42E (red), M42S (green), M42T (blue), M42C (cyan), and M42Q (magenta). Panel C: Wild type (black), M42H (red), M42W (green), and M42Y (blue). Solid lines represent the theoretical fits to a two-state unfolding model with the parameter values listed in Table 1 (see "MATERIALS AND METHODS").

Thermal Unfolding—Figure 5 shows the temperature dependence of the molar ellipticity at 222 nm and the fluorescence intensity at 345 nm of the wild-type and M42V DHFRs at pH 7.0. As shown in Fig. 5A, the molar ellipticity of the wild type increased gradually with temperature in the range 5–50°C and then rapidly in the range 50–70°C to almost constant values at 70–80°C. The fluorescence intensity of the wild type decreased gradually in the range 5–30°C, remained constant at 30–45°C, then decreased again with increasing temperature (Fig. 5B). These results are consistent with our previous conclusion that the thermal unfolding of the wild-type DHFR follows a three-state unfolding model with one intermediate (*21*). However, the molar ellipticity of M42V showed only a small temperature dependence in the range 5–40°C, and then increased rapidly in the transition region at 40–55°C to reach saturation at 55–65°C (Fig. 5A). The fluorescence intensity of M42V also showed a clear transition in the same temperature region (Fig. 5B), indicating that the thermal unfolding of M42V essentially follows a two-state unfolding model. The thermodynamic parameters obtained from the CD data using Eqs. 1 and 2 were T_m = 45.5 ± 0.2°C, ΔH_m = 70.9 ± 2.4 kcal·mol^{-1}, and ΔC_p = 1.4 ± 1.2 kcal·mol^{-1}·K^{-1}. Although these parameters were not obtained for the wild type, the thermal stability of M42V is evidently lower than that of the wild type. Besides the different thermal unfolding mechanism, the native structures of both DHFRs differ considerably in their susceptibility to thermal fluctuation as revealed by the temperature dependence of molar ellipticity, although the thermally unfolded state has an identical structure as shown in the inset of Fig. 5A.

Equilibrium Unfolding—Figure 6 shows typical plots of the molar ellipticities at 222 nm of the wild-type and mutant DHFRs as a function of urea concentration at 15°C. The transition curves of mutant DHFRs were obviously shifted from that of the wild type to lower urea concentrations, suggesting that these mutants have a destabilized structure. However, the slopes of the transition curves are also dependent on the mutants, with gentle slopes being observed for M42P and M42W. The unfolding of the mutant DHFRs essentially follows a two-state

Table 1. **Thermodynamic parameters for urea denaturation of the wild-type and mutant DHFRs at 15°C.**[a]

DHFR	$\Delta g°_{tr}$ [b] (kcal·mol^{-1})	V [c] (ml·mol^{-1})	$\Delta G°_{u}$ [d] (kcal·mol^{-1})	m [d] (kcal·mol^{-1}·M^{-1})	C_m [d] (M)
Wild type [e]	1.3	124	6.08 ± 0.18	–1.96 ± 0.06	3.11
M42E	–2.5	109	3.07 ± 0.28	–1.96 ± 0.15	1.57
M42S	–0.3	73	4.50 ± 0.29	–1.86 ± 0.11	2.42
M42Q	–0.2	114	4.37 ± 0.22	–2.06 ± 0.10	2.12
M42G	0	48	4.40 ± 0.50	–2.28 ± 0.24	1.93
M42T	0.4	93	2.90 ± 0.39	–1.53 ± 0.17	1.90
M42A	0.5	67	5.75 ± 0.54	–2.45 ± 0.22	2.35
M42H	0.5	118	3.06 ± 0.43	–1.95 ± 0.22	1.57
M42P	1.0	90	4.78 ± 1.10	–1.46 ± 0.36	3.27
M42C	1.0	86	4.81 ± 0.26	–2.10 ± 0.11	2.29
M42V	1.5	105	5.04 ± 0.38	–2.09 ± 0.15	2.41
M42L	1.8	124	5.34 ± 0.51	–2.12 ± 0.19	2.52
M42I	1.8	124	5.85 ± 0.58	–2.17 ± 0.21	2.70
M42Y	2.3	141	6.40 ± 0.48	–2.55 ± 0.18	2.51
M42W	3.5	163	4.17 ± 0.40	–1.45 ± 0.14	2.88

[a]The solvent used was 10 mM potassium phosphate (pH 7.0) containing 0.1 mM EDTA and 0.1 mM dithiothreitol. [b]The change in transfer free energy of introduced amino acid side chains from organic solvent to water (*33*). [c]Molar volume of amino acids (*34*). [d]The parameters $\Delta G°_{u}$, m, and C_m were calculated assuming a linear relationship between ΔG_u and the urea concentration (Eq. 3). The values are given as mean ± SD. [e]Gekko *et al.* (*4*).

model, as in the case of the wild-type and other mutant DHFRs, so the change in free energy with unfolding, ΔG_u, was calculated using Eq. 1. The highly linear relationship observed between ΔG_u and urea concentration (data not shown) allows us to calculate the change in free energy with unfolding in water, $\Delta G°_{u}$, the slope, m, and the denaturant concentration at $\Delta G_u = 0$, C_m. The results of the calculation are listed in Table 1. Evidently, the mutations induce large variations in $\Delta G°_{u}$ (2.90–6.40 kcal·mol^{-1}), C_m (1.57–3.27 M), and m (–1.45 to –2.55 kcal·mol^{-1}·M^{-1}) relative to the corresponding values for the wild type (6.08 kcal·mol^{-1}, 3.10 M, and –1.96 kcal·mol^{-1}·M^{-1}, respectively). These results clearly indicate that position 42 plays an important role in the structural stability of the enzyme.

Table 2. **Steady-state kinetic parameters of the enzyme activity of the wild-type and mutant DHFRs at 25°C.**[a]

DHFR	K_m (μM)	k_{cat} (s^{-1})	k_{cat}/K_m (μM^{-1}·s^{-1})
Wild type [b]	1.30 ± 0.10	24.6 ± 3.1	18.9
M42E	5.97 ± 0.69	15.9 ± 0.4	2.7
M42S	2.27 ± 0.16	22.6 ± 0.6	10.0
M42Q	2.27 ± 0.20	24.3 ± 0.8	10.7
M42G	1.18 ± 0.12	13.0 ± 0.4	11.0
M42T	0.82 ± 0.07	18.7 ± 0.4	22.8
M42A	1.30 ± 0.19	14.0 ± 0.8	10.8
M42H	1.93 ± 0.32	26.6 ± 1.5	13.8
M42P	0.83 ± 0.14	24.0 ± 1.1	28.9
M42C	1.94 ± 0.24	30.4 ± 1.2	15.7
M42V	0.91 ± 0.14	15.7 ± 0.7	17.3
M42L	1.12 ± 0.13	18.9 ± 0.6	16.9
M42I	0.61 ± 0.11	12.4 ± 0.5	20.3
M42Y	1.78 ± 0.15	45.5 ± 1.3	25.6
M42W	45.0 ± 2.55	104.6 ± 2.3	2.3

[a]The solvent used was 33 mM succinic acid containing 44 mM imidazole and 44 mM diethanolamine (pH 7.0). [b]Ohmae *et al.* (*6*).

Steady-State Kinetics—Figure 7 shows typical plots of the initial velocity of the enzyme reaction as a function of substrate concentration (DHF). Similar hyperbolic curves were observed for other mutant DHFRs, although for M42W, the curve saturated at a much higher substrate concentration. The Michaelis constant, K_m, and the rate constant of catalysis, k_{cat}, were calculated using Eq. 4 and are listed in Table 2. The K_m values of the mutants other than M42W varied from 0.61 μM (M42I) to 5.97 μM (M42E), and the k_{cat} values varied from 12.4 s^{-1} (M42I) to

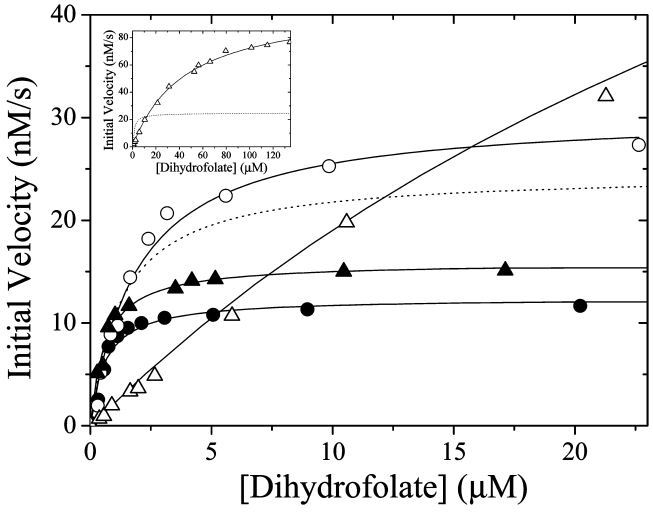

Fig. 7. **Initial velocity of the enzymatic reaction of the four mutant DHFRs as a function of dihydrofolate concentration at 25°C and pH 7.0.** The solvent used was 33 mM succinic acid, 44 mM imidazole, and 44 mM diethanolamine (pH 7.0), containing 60 μM NADPH. The concentrations of enzymes were 0.5–1.5 nM: M42C (open circles), M42l (solid circles), M42W (open triangles), and M42E (solid triangles). Solid lines represent the theoretical fits to Eq. 4 with the parameter values listed in Table 2. The dotted line indicates the theoretical values of the wild-type DHFR.

Table 3. **Equilibrium dissociation constants of NADPH and folate from the wild-type and M42W DHFRs at 25°C and pH 7.0.**[a]

DHFR	K_d (μM)	
	NADPH	Folate
Wild type	0.1 ± 0.0	2.0 ± 0.1
M42W	0.5 ± 0.1	21.8 ± 1.3

[a]The solvent used was 10 mM potassium phosphate (pH 7.0) containing 0.1 mM EDTA and 0.1 mM dithiothreitol.

45.5 s^{-1} (M42Y). M42W shows exceptionally high values of K_m (45.0 μM) and k_{cat} (104.6 s^{-1}), suggesting modified enzyme kinetics. These kinetic parameters for the mutant enzymes differ considerably from the corresponding values for the wild-type DHFR (1.30 μM and 18.9 s^{-1}), but the enzyme activity (k_{cat}/K_m) did not change greatly due to compensation between k_{cat} and K_m in all mutants. Thus the mutation at site 42 has no crucial effect on the function of the enzyme, although the rate-limiting process might be modified (*11*).

Equilibrium Dissociation Constants—Figure 8 shows the concentration dependence of NADPH and folate on the fluorescence intensities at 345 nm of the wild-type and M42W DHFRs at 25°C and pH 7.0. Evidently, the introduction of a tryptophan residue at site 42 influences the affinity for folate and NADPH. The equilibrium dissociation constants of these ligands were calculated using Eq. 5 and are listed in Table 3. The mutations induced 5- and 11-fold increases in the K_d values for NADPH and folate, respectively. Rajagopalan *et al*. (*11*) also found that M42W exhibits 3- and 13-fold higher K_d values for $NADP^+$ and THF, respectively, compared with the wild type. These results suggest that the affinities for coenzyme and substrate are significantly depressed in M42W, although a direct comparison of K_d values is impossible because of the different solvent conditions and ligands used.

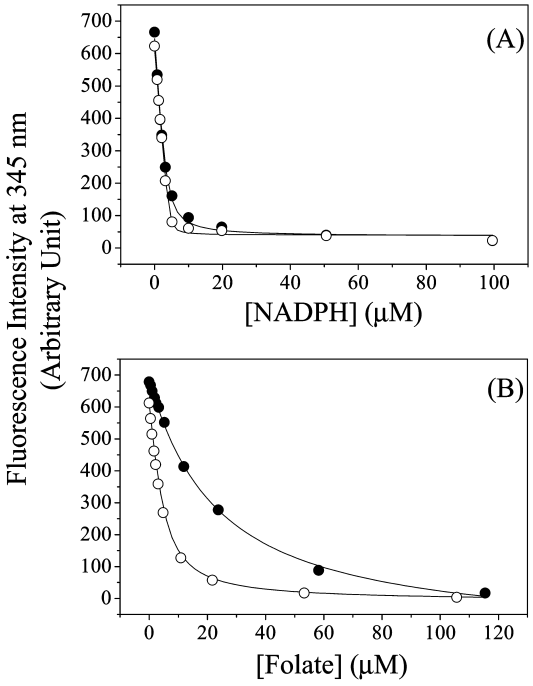

Fig. 8. **NADPH (A) and folate (B) concentration dependence of the fluorescence intensity at 345 nm of the wild-type and M42W DHFRs at 25°C and pH 7.0.** The solvent used was 10 mM potassium phosphate (pH 7.0) containing 0.1 mM EDTA and 0.1 mM dithiothreitol: wild type (open circles) and M42W (solid circles). Solid lines represent the theoretical fits to Eq. 5 with the parameter values listed in Table 3.

DISCUSSION

The present study revealed that mutations at site 42 induce significant changes in the structure, stability, and function of DHFR. This is in agreement with the evolutional evidence that residues 41–45 (including this site) are tightly conserved in DHFRs of many species (*11*). The influence of distal yet highly conserved sites has been demonstrated previously for sites 67 and 121, which are located in flexible loops (*4–6*). It is of interest how local structural changes at distal residues are coupled to the overall structure, stability, and function of the protein. This problem is discussed below in terms of the correlation with the characteristics of the introduced amino acids.

Structure of Mutant DHFRs—As shown in Fig. 2, the CD spectra of mutant DHFRs at site 42 differed significantly from that of the wild type. To our knowledge, this is the first observation of such a large CD change at around 230 nm, although similar CD perturbations have been found for some mutants at tryptophan residues, loops, and hinge regions of DHFR (*6*, *15*, *19*, *22*). It is generally thought that CD spectra in the far-ultraviolet region reflect the secondary structure of a protein. However, the tertiary structure, especially the side chains of aromatic residues, is known to influence the peptide CD of some proteins (*23*, *24*). A typical case is exciton coupling between the Trp47 and Trp74 side chains of DHFR, which has been predicted both experimentally and theoretically (*20*, *25*). Since all the mutants examined in the present study exhibited activities comparable to that of the wild type (Table 2), the observed changes in CD spectra could be ascribed to modifications of exciton coupling between Trp47 and Trp74 rather than to modifications in the secondary structure. It is possible that mutations at site 42 influence the surroundings of the side chain of Trp47, thereby disrupting exciton coupling with Trp74, because the distance between the sulfur atom of Met42 and the nearest atom of Trp47 (α-carbon) is only 3.73 Å, and the side chain of Met42 is buried in the interior of the protein molecule (Fig. 1B). Evidence for such modified exciton coupling is provided by the CD intensity at around 230 nm, and by the fact that the fluorescence intensity increases with increases in the volume or hydrophobicity of the introduced amino acids with aliphatic side chains (Figs. 2A and 4A). Polar and acidic side chains may also disturb the exciton coupling in a more complicated manner, since the order of increasing CD intensity at around 230 nm is not necessarily consistent with that of the fluorescence intensity, as shown in Figs. 2B and 4B. It is noticeable that some mutants (*e.g.*, M42I and M42Q) have a clearly higher CD intensity at around 230 nm compared with W74L, W74F, and W47L, whose exciton coupling is broken. This suggests that the mutants with a high CD intensity induce a new exciton

that differs from that in the wild type. Such modified exciton coupling returns to the state in the wild type by binding a substrate, folate, as demonstrated for M42I (Fig. 3). The symmetric change in the CD intensities centered at about 225 nm as shown in Fig. 3 is further evidence for the modification of exciton coupling. On the other hand, three mutants with aromatic side chains (M42H, M42Y, and M42W) exhibit CD spectra resembling those of W74L, W74F, and W47L (Fig. 2C). The high fluorescence intensity of these mutants (Fig. 4C) suggests that the fluorescence of Trp47, which is quenched in the wild type, is released by introducing these aromatic side chains into site 42 to disrupt the exciton coupling between Trp47 and Trp74.

The disruption of exciton coupling between Trp47 and Trp74 has also been observed in the acid and thermal unfolding intermediate of the wild type (*21*). It is probable that M42V and maybe some other mutant DHFRs in which exciton coupling is disrupted have structures similar to that of the thermal unfolding intermediate of the wild type, and that the increased fluorescence in the intermediate is derived from Trp47.

In contrast to other mutants, M42P exhibits a blue-shifted CD spectrum with a low intensity and without a detectable band at 230 nm compared with the wild type (Fig. 2A). Some conformational change might occur by introducing a proline residue, since site 42 is located in a short β-strand and the solubility of this mutant is very low compared with that of the other mutants. Although elucidation of the detailed structural changes must await X-ray or NMR analyses of the mutant enzymes, the present spectroscopic data reveal that mutations at site 42 have little effect on the secondary structure, but strongly perturb the tertiary structure of DHFR.

Structural Stability—As indicated in Table 1, the $\Delta G°_u$ values of all mutants except M42Y are lower than that of the wild type, indicating that mutations at site 42 mainly destabilize the structure of DHFR. This is consistent with the comparable decrease in the C_m values (correlation coefficient, r, between $\Delta G°_u$ and C_m is 0.672). From thermodynamics, it is difficult to determine *a priori* which of the native and unfolded structures modifies the stability of mutants. However, a linear correlation between $\Delta G°_u$ and m (r = –0.565) suggests that the cooperativity of unfolding or the flexibility of the native structure may also be related to the stability of the protein, although interpretations of the m value remain controversial (*26*, *27*). The CD data in Figs. 2, 5, and 6 clearly indicate that the mutations affect the native structure more than the unfolded structure.

The stabilizing mechanism of a protein can be partly understood through the correlation of $\Delta G°_u$ with structural parameters of the introduced amino acid residues. Many experimental data indicate that $\Delta G°_u$ increases with increases in the hydrophobicity of introduced amino acid side chains (*28–31*), leading to a consensus that hydrophobic interactions represent the dominant stabilizing force of protein structure (*32*). This is also expected for the mutants in the present study since the side chain of Met42 (wild type) is buried in the interior of the protein molecule. Therefore, the $\Delta G°_u$ values in Table 1 are plotted in Fig. 9A as a function of the hydrophobicity ($\Delta g°_{tr}$) of the introduced amino acid side chains, as estimated by Nozaki and Tanford (*33*). Evidently, $\Delta G°_u$ is an increasing function of $\Delta g°_{tr}$, although the correlation is not high (r = 0.518). As shown in Fig. 9B, a stronger positive correlation is observed between C_m and $\Delta g°_{tr}$ (r = 0.647). Therefore, the mutation effects on stability can be attributed mainly to enhanced hydrophobic interactions in the native structure. The side chains with high hydrophobicity concomitantly have large molar volumes, so a packing effect of the side chains may be also related to the stability of the mutants. However, there is no significant correlation between the molar volume of the introduced amino acid residues (V) and $\Delta G°_u$ (r = 0.135) or C_m (r = 0.285) (data not shown), although overcrowding of side chains dominantly contributes to the stability of mutants at sites 67 and 121 in loop regions, whose side chains are also buried in the protein molecule (*4*, *6*). Therefore, atomic packing of the side chains is not so significant as overcoming the effect of hydrophobicity on the stability of mutants at site 42.

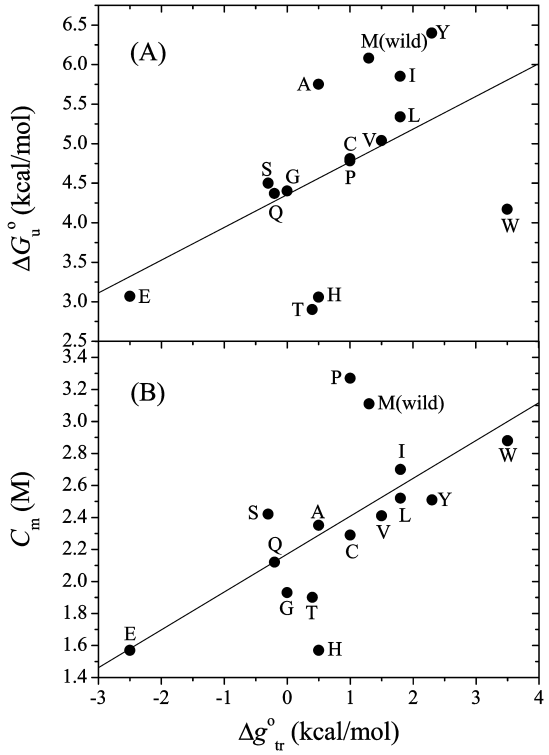

Fig. 9. **Plots of $\Delta G°_u$ (A) and Cm (B) against the hydrophobicity ($\Delta g°_{tr}$) of introduced amino acid side chains for the wild-type and mutant DHFRs.** The hydrophobicity values are from Nozaki and Tanford (*33*). Amino acid residues at site 42 are indicated as one-letter codes. Solid lines represent linear regressions.

The thermal stability of DHFR is also influenced by mutations at site 42, as demonstrated for M42V in Fig. 5. The stability change is mainly attributable to the modified native structure. It is possible that the thermal stability of other mutants is influenced by the hydrophobicity of the introduced amino acids as in the case of urea denaturation, although confirmation of this awaits detailed thermodynamic analyses.

Enzyme Function—As indicated in Table 2, the steady-state kinetic parameters of mutant DHFRs at site 42 differ considerably from those of the wild type, especially

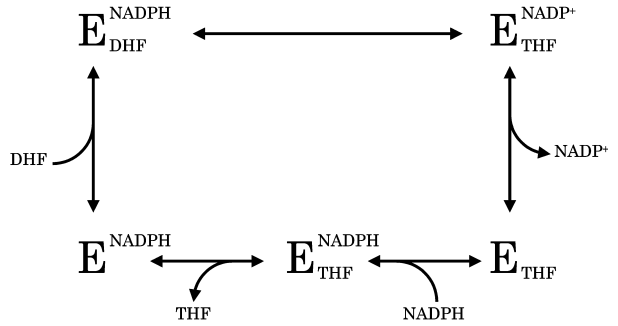

Scheme 1.

M42W, which has significantly higher K_m and k_{cat} values. This is interesting because the mutation site is far (14 Å) from the active site (Asp27) and hence has no direct contact with either the substrate or cofactor. DHFR catalyzes the NADPH-linked reduction of DHF to THF through a cyclic reaction pathway consisting of five intermediates (DHFR-NADPH, DHFR-NADPH-DHF, DHFR-NADP$^+$-THF, DHFR-THF, and DHFR-NADPH-THF), and involves some equilibrium states such as DHFR-NADP$^+$ (Scheme 1) (*14*).

In the cycle shown in Scheme 1, the ternary complex DHFR-NADPH-DHF exists only transiently because the hydride transfer from NADPH to DHF is very rapid. The movie produced by Sawaya and Kraut (*1*) indicates that DHFR actively and cooperatively fluctuates in the binding and releasing of these ligands. For the wild type, the rate-limiting step in this cycle is the release of a product, THF (*14*), so we cannot explain the mutation effects on the total enzyme kinetics by considering only the K_m and k_{cat} values. However, it is possible to predict the characteristics of mutations at site 42 from the correlation of these kinetic parameters with the nature of the amino acids introduced.

Figure 10 shows plots of K_m, k_{cat}, and log (k_{cat}/K_m) as a function of the hydrophobicity ($\Delta g°_{tr}$) of the introduced amino acid side chains. Except for M42W, it appears that K_m decreases (r = –0.804) and k_{cat} increases (r = 0.351) with increasing $\Delta g°_{tr}$, resulting in the increase in k_{cat}/K_m (r = 0.885). The large reduction (seven-fold) in enzyme activity (k_{cat}/K_m) of M42E may be attributable to its side chain having the highest polarity, which may be exposed with a negative charge to the solvent. As shown in Fig. 1B, the side chain of Met42 is close to that of Ile50, which comes directly into contact with the *p*-aminobenzoyl moiety of the substrate. So it is possible that the introduction of a hydrophilic side chain into site 42 disrupts the hydrophobic interaction with the side chain of Ile50, consequently decreasing the affinity for the substrate. Thus the side-chain hydrophobicity at site 42 would enhance the enzyme function mainly by increasing the affinity for the substrate.

However, M42W shows exceptionally low activity (8.2-fold) comparable to that of M42E, although its side chain is the most hydrophobic of all the amino acids. Such depressed activity is mainly attributable to the reduced substrate binding (35-fold increase in K_m) overcoming the decrease in the turnover reaction rate (4.3-fold increase in k_{cat}). This is supported by the equilibrium dissociation

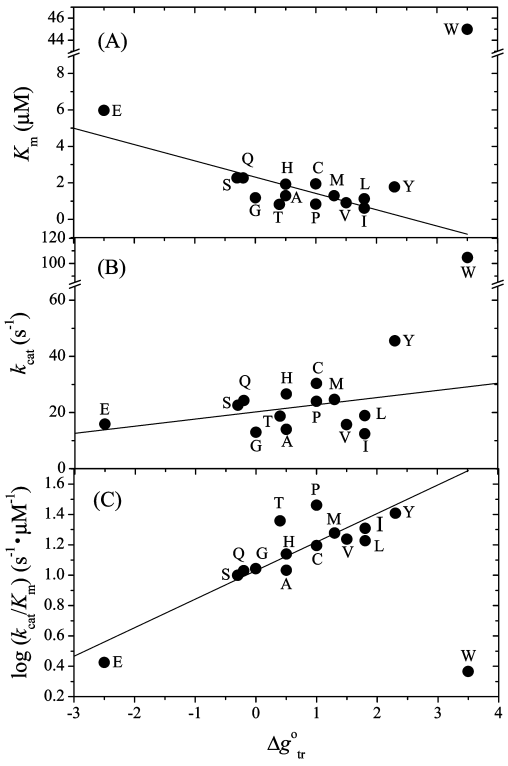

Fig. 10. **Plots of K_m (A), k_{cat} (B), and log k_{cat}/K_m (C) against the hydrophobicity ($\Delta g°_{tr}$) of introduced amino acid side chains for the wild-type and mutant DHFRs.** The hydrophobicity values are from Nozaki and Tanford (*33*). Amino acid residues at site 42 are indicated as one-letter codes. Solid lines represent linear regressions, except for the M42W mutant.

constant of folate for M42W being 11-fold higher than that of the wild type (Table 3). On the other hand, Rajagopalan *et al*. (*11*) found that the dissociation constants of M42W and M42F for the substrate (DHF) and coenzyme (NADPH) are comparable to those of the wild type, but that the forward hydride-transfer rate of M42W was reduced 41-fold while the reaction kinetics of the M42F mutant did not deviate from the wild-type behavior. Furthermore, in the M42W mutant, the dissociation rate of THF from the reduced ternary complex (DHFR-NADPH-THF) increased 13-fold relative to the wild type, and hydride transfer was likely to be the rate-limiting step. They also predicted that the kinetically significant conformational-change step would precede the chemical step between DHFR-NADPH-DHF and DHFR-NADP$^+$-THF (Scheme 1) in M42W, resembling that previously observed for G121V (*5*). Thus, on scaling with side-chain hydrophobicity, M42W has specific enzyme kinetics that differ from those of the wild-type and other mutant DHFRs.

As revealed by the present study, site 42 distal to the active site plays an important role in the stability and function of DHFR. The main effect of the mutations is the modification of hydrophobic interactions with residues surrounding this position, as expected from the wide-type side chain being buried in the hydrophobic core. We are currently using mass spectrometry to investigate the hydrogen–deuterium exchange of these mutants coupled

with protease digestion, which should provide further insight into the role of site 42 in the structure–fluctuation–function relationship.

REFERENCES

1. Sawaya, M.R. and Kraut, J. (1997) Loop and subdomain movements in the mechanism of *Escherichia coli* dihydrofolate reductase: crystallographic evidence. *Biochemistry* **36**, 586–603
2. Kitahara, R., Sareth, S., Yamada, H., Ohmae, E., Gekko, K., and Akasaka, K. (2000) High pressure NMR reveals active-site hinge motion of folate-bound *Escherichia coli* dihydrofolate reductase. *Biochemistry* **39**, 12789–12795
3. Gekko, K., Yamagami, K., Kunori, Y., Ichihara, S., Kodama, M., and Iwakura, M. (1993) Effects of point mutation in a flexible loop on the stability and enzymatic function of *Escherichia coli* dihydrofolate reductase. *J. Biochem.* **113**, 74–80
4. Gekko, K., Kunori, Y., Takeuchi, H., Ichihara, S., and Kodama, M. (1994) Point mutations at glycine-121 of *Escherichia coli* dihydrofolate reductase: important roles of a flexible loop in the stability and function. *J. Biochem.* **116**, 34–41
5. Cameron, C.E. and Benkovic, S.J. (1997) Evidence for a functional role of the dynamics of glycine-121 of *Escherichia coli* dihydrofolate reductase obtained from kinetic analysis of a site-directed mutant. *Biochemistry* **36**, 15792–15800
6. Ohmae, E., Iriyama, K., Ichihara, S., and Gekko, K. (1996) Effects of point mutations at the flexible loop glycine-67 of *Escherichia coli* dihydrofolate reductase on its stability and function. *J. Biochem.* **119**, 703–710
7. Ohmae, E., Ishimura, K., Iwakura, M., and Gekko, K. (1998) Effects of point mutations at the flexible loop alanine-145 of *Escherichia coli* dihydrofolate reductase on its stability and function. *J. Biochem.* **123**, 839–846
8. Ohmae, E., Iriyama, K., Ichihara, S., and Gekko, K. (1998) Nonadditive effects of double mutations at the flexible loops, glycine-67 and glycine-121, of *Escherichia coli* dihydrofolate reductase on its stability and function. *J. Biochem.* **123**, 33–41
9. Gekko, K., Kamiyama, T., Ohmae, E., and Katayanagi, K. (2000) Single amino acid substitutions in flexible loops can induce large compressibility changes in dihydrofolate reductase. *J. Biochem.* **128**, 21–27
10. Yamamoto, T., Izumi, S., Ohmae, E., and Gekko, K. (2004) Mass spectrometry of hydrogen/deuterium exchange of *Escherichia coli* dihydrofolate reductase: effects of loop mutations. *J. Biochem.* **135**, 487–494
11. Rajagopalan, P.T.R., Lutz, S., and Benkovic, S.J. (2002) Coupling interactions of distal residues enhance dihydrofolate reductase catalysis: mutational effects on hydride transfer rates. *Biochemistry* **41**, 12618–12628
12. Shaw, D., Odom, J.D., and Dunlap R.B. (1999) High expression and steady-state kinetic characterization of methionine site-directed mutants of *Escherichia coli* methionyl- and selenomethionyl-dihydrofolate reductase. *Biochim. Biophys. Acta* **1429**, 401–410
13. Iwakura, M., Jones, B.E., Luo, J., and Matthews, C.R. (1995) A strategy for testing the suitability of cysteine replacements in dihydrofolate reductase gene from *Escherichia coli*. *J. Biochem.* **117**, 480–488
14. Fierke, C.A., Johnson, K.A., and Benkovic, S.J. (1987) Construction and evaluation of the kinetic scheme associated with dihydrofolate reductase from *Escherichia coli*. *Biochemistry* **26**, 4085–4092
15. Ohmae, E., Sasaki, Y., and Gekko, K. (2001) Effects of five-tryptophan mutations on structure, stability and function of *Escherichia coli* dihydrofolate reductase. *J. Biochem.* **130**, 439–447
16. Pace, C.N. (1985) Determination and analysis of urea and guanidine hydrochloride denaturation curves in *Methods Enzymol.* (Hirs, C.H.W. and Timasheff, S.N., eds.) Vol. **131**, pp. 267–280, Academic Press, New York
17. Williams, J.W., Morrison, J.F., and Duggleby, R.G. (1979) Methotrexate, a high-affinity pseudosubstrate of dihydrofolate reductase. *Biochemistry* **18**, 2567–2573
18. Penner, M.H. and Frieden, C. (1985) Substrate induced hysteresis in the activity of *Escherichia coli* dihydrofolate reductase. *J. Biol. Chem.* **260**, 5366–5369
19. Stone, S.R. and Morrison, J.F. (1982) Kinetic mechanism of the reaction catalyzed by dihydrofolate reductase from *Escherichia coli*. *Biochemistry* **21**, 3757–3765
20. Kuwajima, K., Garvey, E.P., Finn, B.E., Matthews, C.R., and Sugai, S. (1991) Transient intermediates in the folding of dihydrofolate reductase as detected by far-ultraviolet circular dichroism spectroscopy. *Biochemistry* **30**, 7693–7703
21. Ohmae, E., Kurumiya, T., Makino, S., and Gekko, K. (1996) Acid and thermal unfolding of *Escherichia coli* dihydrofolate reductase. *J. Biochem.* **120**, 946–953
22. Ahrweiler, P.M. and Frieden, C. (1991) Effects of point mutations in a hinge region on the stability, folding, and enzymatic activity of *Escherichia coli* dihydrofolate reductase. *Biochemistry* **30**, 7801–7809
23. Arnold, G.E., Day, L.A., and Dunker, A.K. (1992) Tryptophan contributions to the unusual circular dichroism of fd bacteriophage. *Biochemistry* **31**, 7948–7956
24. Vuilleumier, S., Sancho, J., Loewenthal, R., and Fersht, A.R. (1993) Circular dichroism studies of barnase and its mutants: characterization of the contribution of aromatic side chains. *Biochemistry* **32**, 10303–10313
25. Grishina, I.B. and Woody, R.W. (1994) Contributions of tryptophan side chains to the circular dichroism of globular proteins: exciton couplets and coupled oscillators. *Faraday Discuss.* **99**, 245–262
26. Shellman, J.A. (1978) Solvent denaturation. *Biopolymers* **17**, 1305–1322
27. Pace, C.N., Laurents, D.V., and Thomson, J.A. (1990) pH dependence of the urea and guanidine hydrochloride denaturation of ribonuclease A and ribonuclease T1. *Biochemistry* **29**, 2564–2572
28. Yutani, K., Ogasahara, K., Tsujita, T., and Sugino, Y. (1987) Dependence of conformational stability on hydrophobicity of the amino acid residue in a series of variant proteins substituted at a unique position of tryptophan synthase α subunit. *Proc. Natl Acad. Sci. USA* **84**, 4441–4444
29. Matsumura, M., Becktel, W.J., and Matthews, B.W. (1988) Hydrophobic stabilization in T4 lysozyme determined directly by multiple substitutions of Ile 3. *Nature* **334**, 406–410
30. Matsumura, M., Yahanda, S., Yasumura, S., Yutani, K., and Aiba, S. (1988) Role of tyrosine-80 in the stability of kanamycin nucleotidyltransferase analyzed by site-directed mutagenesis. *Eur. J. Biochem.* **171**, 715–720
31. Kellis, J.T. Jr., Nyberg, K., and Fersht, A.R. (1989) Energetics of complementary side-chain packing in a protein hydrophobic core. *Biochemistry* **28**, 4914–4922
32. Kauzmann, W. (1959) Some factors in the interpretation of protein denaturation. *Adv. Protein Chem.* **14**, 1–63
33. Nozaki, Y. and Tanford, C. (1971) The solubility of amino acids and two glycine peptides in aqueous ethanol and dioxane solutions. Establishment of a hydrophobicity scale. *J. Biol. Chem.* **246**, 2211–2217
34. Zamyatnin, A.A. (1984) Amino acid, peptide, and protein volume in solution. *Annu. Rev. Biophys. Bioeng.* **13**, 145–165
35. Bolin, J.T., Filman, D.J., Matthews, D.A., Hamlin, R.C., and Kraut, J. (1982) Crystal structures of *Escherichia coli* and *Lactobacillus casei* dihydrofolate reductase refined at 1.7 Å resolution. I. General features and binding of methotrexate. *J. Biol. Chem.* **257**, 13650–13662